NANO LETTERS

pubs.acs.org/NanoLett

Letter

Anisotropic Magnon Spin Transport in Ultrathin Spinel Ferrite Thin Films—Evidence for Anisotropy in Exchange Stiffness

Ruofan Li, Peng Li, Di Yi, Lauren J. Riddiford, Yahong Chai, Yuri Suzuki, Daniel C. Ralph,* and Tianxiang Nan*

Cite This: *Nano Lett.* 2022, 22, 1167−1173

Read Online

ABSTRACT: Magnon-mediated spin flow in magnetically ordered insulators enables long-distance spin-based information transport with low dissipation. In the materials studied to date, no anisotropy has been observed in the magnon propagation length as a function of propagation direction. Here, we report measurements of magnon spin transport in a spinel ferrite, magnesium aluminum ferrite $MgAl_{0.5}Fe_{1.5}O_4$ (MAFO), which has a substantial in-plane 4-fold magnetic anisotropy. We observe spin diffusion lengths > 0.8 μm at room temperature in 6 nm films, with spin diffusion lengths 30% longer along the easy axes compared to the hard axes. The sign of this difference is opposite to the effects just of anisotropy in the magnetic energy for a uniform magnetic state. We suggest instead that accounting for anisotropy in exchange stiffness is necessary to explain these results. These findings provide an approach for controlling magnon transport via strain, which opens new opportunities for designing magnonic devices.

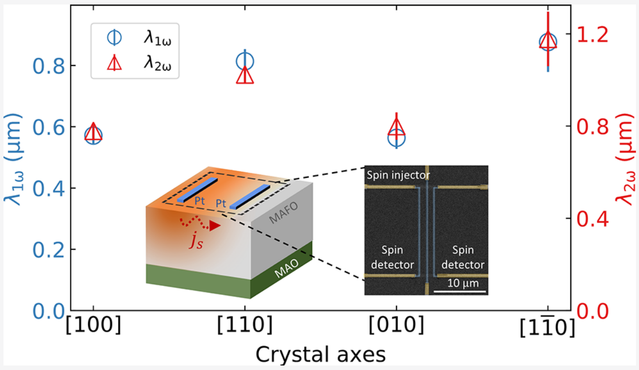

KEYWORDS: *spintronics, magnon transport, spinel ferrite, thin films, exchange stiffness*

INTRODUCTION

Using magnons, the quanta of spin waves, for information transmission offers the potential for low energy dissipation compared to traditional electronic transport.[1] Magnon spin transport has been demonstrated experimentally in both insulating ferrimagnets[2−15] and antiferromagnets.[16−18] The magnon spin diffusion length, the characteristic propagation length, has been studied under various conditions of temperature,[11,19−21] magnon chemical potential,[22−24] external magnetic field,[11,21,25] and magnon drift current.[15] Previous measurements on ferrimagnetic insulators have focused on YIG, either with thick films (>100 nm) which are fully relaxed relative to the substrate[3,5,21] or with thinner films.[15,26] In either case, YIG has very weak magnetic anisotropy, and no anisotropies have been observed in the spin transport.

Here, we report measurements of magnon transport in a low-loss spinel material that has been recently stabilized in epitaxial thin-film form, magnesium aluminum ferrite $MgAl_{0.5}Fe_{1.5}O_4$ (MAFO).[27−31] When grown epitaxially on a $MgAl_2O_4$ substrate, MAFO possesses a substantial in-plane cubic anisotropy (~13 mT with easy axes in the <110> directions), while maintaining low magnetic damping into the regime of ultrathin films. We report that magnon spin transport depends strongly on the propagation direction relative to the anisotropy axes, with a spin diffusion length 30% greater for magnon propagation along the easy axes compared to the hard axes. We argue that this difference has the wrong sign to be explained taking into account only the usual magnetic anisotropy energy which applies to spatially uniform states, but requires also a consideration of anisotropy in the exchange stiffness for nonuniform states. Our results suggest that spin transport measurements can be used as a sensitive probe of the exchange stiffness and that manipulation of this stiffness (e.g., via strain) provides an alternative strategy for controlling magnon spin diffusion.

RESULTS

We employ a measurement geometry commonly used for measuring magnon spin transport—parallel Pt wires with different separation distances deposited on top of the magnetic insulator to be investigated (Figure 1a).[3,5,7,10,11,16,18] The Pt wires have widths of 200 nm, lengths of 10 μm, and spacings that range from 0.4 to 5 μm. A charge current passing through one of the Pt wires results in the excitation of magnons in the magnetic film below the wire by the spin Hall effect (SHE)[32]

Received: November 10, 2021
Revised: January 19, 2022
Published: January 25, 2022

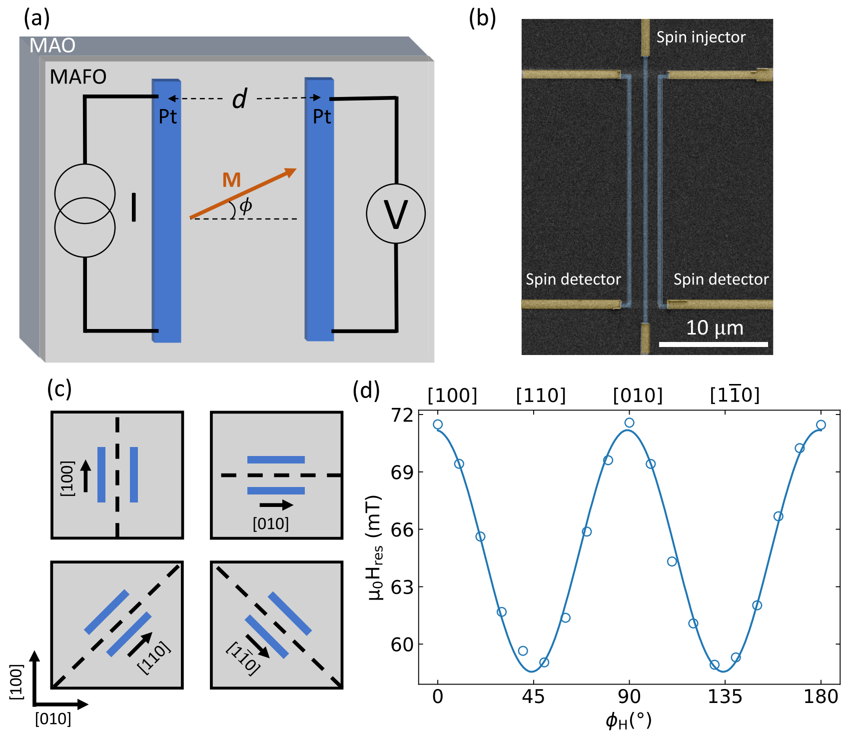

Figure 1. Measurement geometry and magnetic anisotropy of MAFO. (a) Schematic layout of the experimental setup (not to scale). (b) False color scanning electron microscope image of the device, in which blue indicates the Pt wires and yellow corresponds to contact leads. (c) Schematics for measuring magnon transport along different directions relative to the crystal axes of the MAFO film. (d) FMR resonance field at 9 GHz as a function of the angle (ϕ_H) between applied in-plane magnetic field and the [100] crystal axis for a MAFO thin film of 5 nm thickness grown under the same conditions as the 6 nm film. The solid line represents a $\cos(4\phi_H)$ fit to the measured data.

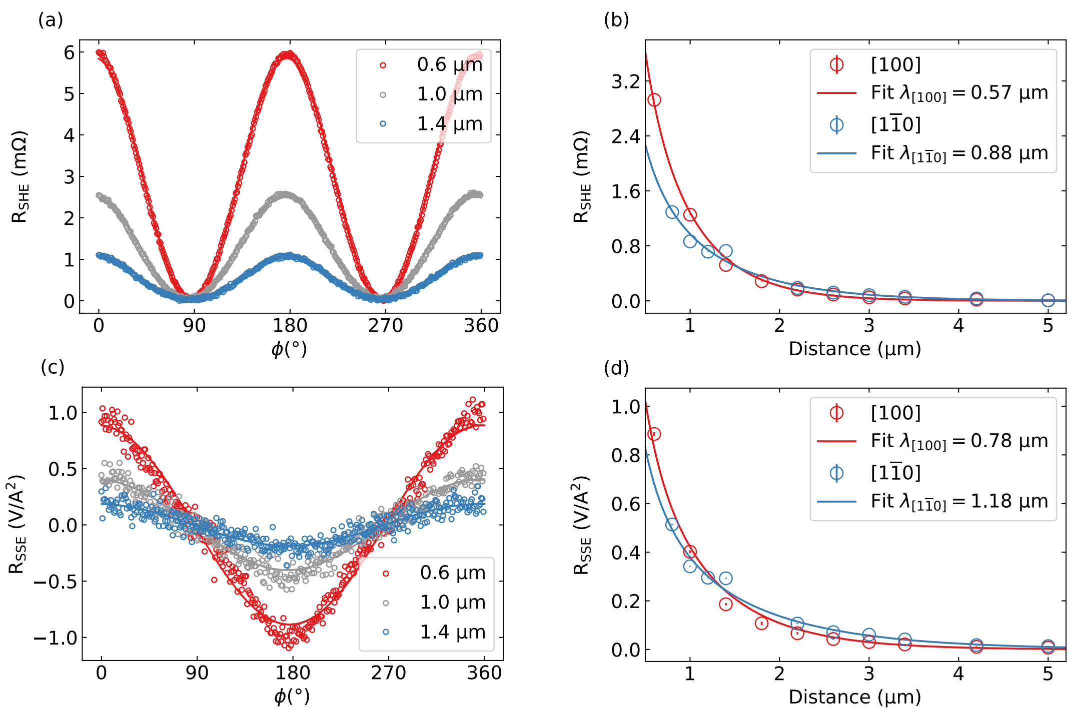

Figure 2. (a) First-harmonic R_{SHE} and (c) second-harmonic R_{SSE} nonlocal signals as functions of the magnetic field angle ϕ for a field magnitude of 75 mT and samples with d = 0.6, 1, and 1.4 μm, with the Pt wires oriented along the [100] direction. Solid lines are the fits to $\cos^2(\phi)$ and $\cos(\phi)$ dependence for first- and second-harmonic signals, respectively. Magnitude of (b) first-harmonic and (d) second-harmonic nonlocal signals as functions of distance between the Pt wires oriented along the [100] and [1$\bar{1}$0] directions. The solid lines are fits to eq 3.

and, because of a thermal gradient arising from Joule heating, also by the spin Seebeck effect (SSE).[33] The excited magnons diffuse through the film to the other Pt wire where they are detected by means of a voltage signal generated by the inverse

https://doi.org/10.1021/acs.nanolett.1c04332
Nano Lett. 2022, 22, 1167−1173

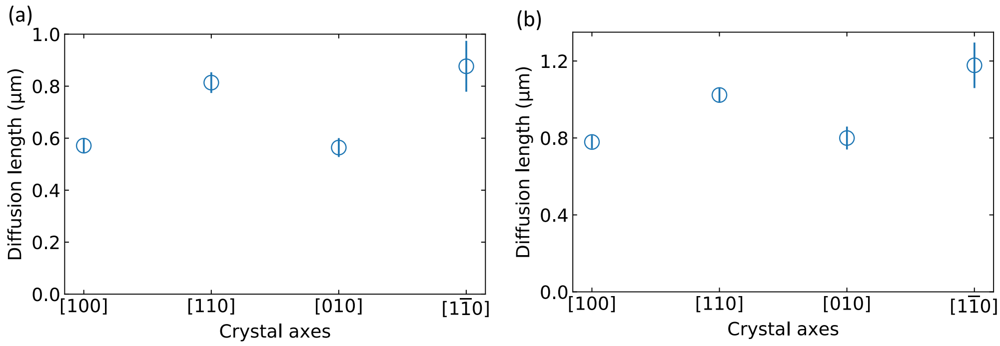

Figure 3. Spin diffusion lengths extracted from the decay of the (a) first- and (b) second-harmonic nonlocal signals for wires along corresponding axes. Error bars represent the standard deviations of the fits.

spin Hall effect (ISHE).[34] Figure 1b shows the scanning electron microscope image of a typical device with the middle Pt wire as the spin injector and the wires on the sides as the spin detectors. To measure magnon spin transport in different directions relative to the underlying crystalline film, we perform measurements on separate devices on the same chip with different orientations of the Pt wires (Figure 1c).

The magnetic insulators we probe are (001)-oriented 6-nm-thick MAFO thin films that are epitaxially grown on $MgAl_2O_4$ (MAO) substrates[27] (see Supporting Information for sample growth and fabrication). Tetragonal distortion due to epitaxial strain acting on MAFO (3% lattice mismatch) induces an in-plane 4-fold magnetic anisotropy with an effective field strength of 13 mT as shown by ferromagnetic resonance (FMR) measurements on a MAFO film of similar thickness (5 nm) grown under the same conditions (Figure 1d). The angular dependence of the anisotropy field is consistent with cubic symmetry, and the easy axes are along <110>. The Gilbert damping in MAFO as measured by FMR remains small and isotropic with respect to the angle of the in-plane magnetic field relative to the crystal axes.[27]

For the magnon spin-transport measurements, we pass a low-frequency current (5.9 Hz) through one Pt wire, exciting magnons in the MAFO film via both the SHE and SSE. All the measurements are performed at room temperature, using different angles and magnitudes of in-plane applied magnetic field and different spacings between the injector and detector Pt wires. The component of the nonlocal voltage (V_{NL}) detected in the distant Pt wire that originates from SHE (V_{SHE}) has a linear dependence on the current (I), while the component from SSE (V_{SSE}), which arises due to a temperature gradient from Joule heating, varies quadratically with I (Figure S4, Supporting Information). These two kinds of nonlocal voltages can therefore be distinguished by detecting the first ($V_{1\omega} = R_{1\omega}I$) and second-harmonic ($V_{2\omega} = R_{2\omega}I^2$) responses using lock-in amplifiers. Depending on their origin, the nonlocal resistances can then be written as

$$R_{1\omega} = R_{SHE} + R_{0,1\omega} \tag{1}$$

$$R_{2\omega} = R_{SSE} + R_{0,2\omega} \tag{2}$$

where R_{SHE} and R_{SSE} represent the nonlocal resistances that we wish to measure arising from the SHE and SSE, while $R_{0,1\omega}$ and $R_{0,2\omega}$ are offset resistances due to inductive and capacitive couplings in the sample and the measurement setup.

To subtract out the constant-impedance parts ($R_{0,1\omega}$ and $R_{0,2\omega}$), we collect $V_{1\omega}$ and $V_{2\omega}$ as a function of the in-plane magnetic angle ϕ for a field magnitude of 75 mT, as shown in Figure 2a. ϕ is defined as the complement of the angle between the magnetization of MAFO and the applied current axis (see Figure 1a). For the electrically generated nonlocal signal V_{SHE}, both the injection and the detection of the magnons have a $\cos(\phi)$ dependence coming from SHE and ISHE, respectively, resulting in a total dependence approximately $\propto \cos^2(\phi)$ (Figure 2a). In the case of the thermally generated nonlocal signal V_{SSE}, the magnon injection is generated by Joule heating, which has no angular dependence, while the detection of the magnons through ISHE varies with angle ϕ, which gives rise to an approximately $\cos(\phi)$ angular dependence (Figure 2c).

Although generally magnon conductance decreases with decreasing thickness in magnetic insulator films due to increased damping,[35] nevertheless, even in 6-nm-thick MAFO films we observe long-range magnon transport across 5 μm gaps. The spin diffusion length can be extracted from the decay of R_{SHE} and R_{SSE} as a function of the separation (d) between the Pt wires (injector and detector). This decay can be well fitted to a magnon diffusion model:[3]

$$R_{NL} = \frac{C}{\lambda} \frac{\exp(d/\lambda)}{1 - \exp(2d/\lambda)} \tag{3}$$

where R_{NL} could be either R_{SHE} or R_{SSE}, C is a distance-independent constant, and λ is an effective spin diffusion length in the direction perpendicular to the Pt wires.

We have investigated the effects of anisotropy by comparing spin diffusion lengths for the orientation of the wires along [100], [110], [010], and [1$\bar{1}$0] axes. Figure 2b shows the first-harmonic nonlocal resistances for the [100] and [1$\bar{1}$0] wire orientations plotted as a function of the wire spacing. The dots in the plots correspond to the experimental data, while the solid lines show the fits to eq 3. A similar decay of the nonlocal resistance vs spacing is also observed for the second-harmonic signal as shown in Figure 2d. The spin diffusion lengths, $\lambda_{1\omega}$ and $\lambda_{2\omega}$, extracted from the fits for first- and second-harmonic signals are shown in Figure 3 for the different crystal-axis orientations.

For both $\lambda_{1\omega}$ and $\lambda_{2\omega}$, we observe significantly larger (>30%) spin diffusion lengths along the <110> axes (easy axes) compared to the <100> axes (hard axes). We also find that the extracted values of $\lambda_{2\omega}$ are slightly larger than $\lambda_{1\omega}$, which has also been observed previously for YIG thin films.[21] This difference can be explained as due to the different mechanisms by which the nonequilibrium magnon distributions are generated for the two signals. Furthermore, due to a lateral thermal gradient near the Pt injector bar, the second-harmonic voltage can have contributions from both local and nonlocal

SSE signals, while for the first-harmonic signal the SHE excites the magnons only locally.[5] The angular dependencies of $\lambda_{1\omega}$ and $\lambda_{2\omega}$ correspond to the same 4-fold symmetry as the in-plane magnetic anisotropy, consistent with the cubic symmetry of MAFO (Figure 1d).

DISCUSSION

If one assumes that the primary cause of anisotropic magnon transport in MAFO is simply the anisotropy in the magnetic energy for a uniform magnetic state, it is surprising that the spin diffusion length is longer in the direction of the magnetic easy axis, rather than the reverse. The magnetic anisotropy energy for a uniform magnetic state should cause the same qualitative behavior as an increased applied magnetic field along the easy axis. Both previous measurements on YIG[21,25] and our own measurements on MAFO (Figure 4a and b) show that the magnitude of the nonlocal spin signal decreases as a function of the increasing magnitude of an applied magnetic field, corresponding to a decreased spin diffusion length with increasing magnetic field. This behavior has been ascribed within the context of the SSE to the influence of the magnetic field increasing the energy of long-wavelength magnons.[25] Quantitatively, the effect of a magnetic field is also far too weak to explain the scale of the effect that we measure. Figure 4a and b both show that a 140 mT magnetic field decreases the spin signal by only 18%, indicating that an in-plane cubic anisotropy of 13 mT could not generate the 30% difference we observe.

The sign of the effect we observe is also surprising within the usual theoretical framework for modeling the energies and group velocities of long-wavelength magnons. The only type of anisotropy that is ordinarily considered is the anisotropy energy for a uniform magnetic state, accounted for in terms of an anisotropy field of 2 $\mu_0 H_{an}$. For a 4-fold in-plane magnetic anisotropy, the dispersion curve for long-wavelength magnons (taking into account both exchange and magnetic dipole contributions) takes the form[36−38]

$$\omega(k, \phi_k, \phi_H) = \frac{g\mu_B}{\hbar}\sqrt{B_1 B_2} \tag{4}$$

with

$$B_1 = B + \mu_0 M_{eff}(1 - P_k) + Dk^2 + \frac{1}{4}\mu_0 H_{an}(3 + \cos(4\phi_H)) \tag{5}$$

$$B_2 = B + \mu_0 M_{eff} P_k \sin^2(\phi_k) + Dk^2 + \mu_0 H_{an} \cos(4\phi_H) \tag{6}$$

and where $k = |\vec{k}|$ is the magnitude of the wavevector, ϕ_k is the angle of the wavevector relative to an easy axis, ϕ_H is the angle of the average magnetization relative to the [100] direction, B = 0.075 T in our angle-dependent measurements, M_{eff} is the saturation magnetization, D is the exchange stiffness, and $P_k = 1 - [(1 - e^{-kd})/(kd)]$ with d as the film thickness. For our MAFO samples, $\mu_0 M_{eff}$ = 1.5 T, $2|\mu_0 H_{an}|$ = 13 mT, and d = 6 nm. For oxide ferrimagnets, a typical value of the exchange stiffness is $D = 5 \times 10^{-17}$ T m^2. The effect of the anisotropy field is to increase the energy of magnons with small values of k for ϕ_k near the easy axis but to cause little change in the energy of magnons with larger k due to the increasing importance of the exchange and dipole terms. As a result, the group velocity, $v_g = d\omega(k, \phi_k, \phi_H)/dk$ is always decreased by an increase in the magnetic anisotropy energy.

This is illustrated in Figure 4c and d, where we plot models of dispersion relations and group velocities for k up to 5×10^8 m^{-1} (a range of k smaller than the full Brillouin zone to make visible the changes in this lower-k regime). The blue line in each panel corresponds to the reasonable parameter values mentioned above, for magnons propagating along the [100] direction of a MAFO film. The orange curve in each panel shows how the dispersion relation and group velocity would change for magnons propagating along the [110] direction, assuming that the only source of anisotropy is the magnetic anisotropy for a uniform magnetic state (associated with the anisotropy field $2|\mu_0 H_{an}|$ = 13 mT). From the difference between blue and orange curves, it can be seen that the group velocity is slightly larger along the hard axis ([100]), although the difference is visible only in a very small portion of the Brillouin zone near k = 0, where the group velocity is already very low. In addition to these small changes in group velocity, a larger value of H_{an} will also decrease the thermal magnon population. Both effects should decrease the spin diffusion length in the direction of a magnetic easy axis.

We therefore draw the conclusion, based on both the sign and magnitude of the effect we observe, that the anisotropic nonlocal spin signal must be caused by crystalline anisotropies which are different from simply the magnetic anisotropy energy for a uniform magnetic state. We considered whether the scattering time for spin relaxation might depend on the orientation of $\vec{k}$ with respect to the anisotropy axes. But if this were the case, we would expect the scattering to also depend on the orientation of $\vec{k}$ with respect to the applied magnetic

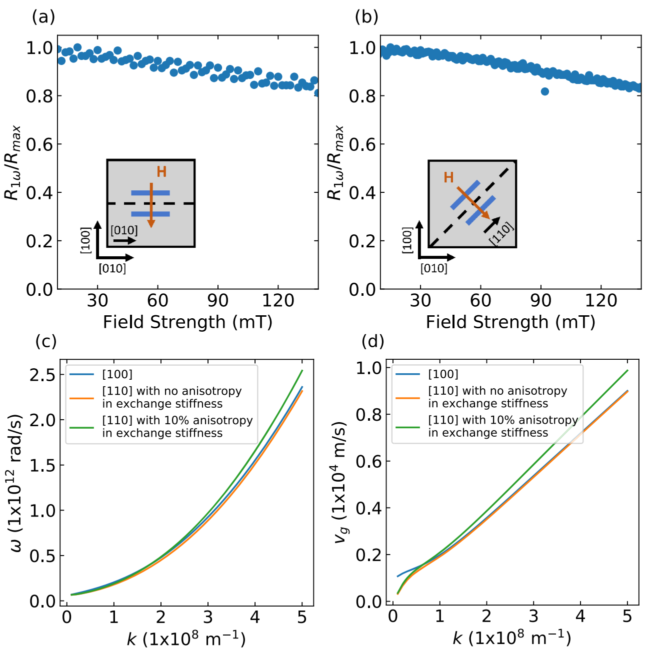

Figure 4. Ratio of the first harmonic nonlocal signal to its maximum value as a function of applied magnetic field at ϕ = 0 for samples with d = 1 μm and Pt wires oriented along (a) the hard axis and (b) the easy axis. The inset in each plot shows the orientation of the Pt wires and applied magnetic field with respect to the crystal axes. (c,d) Dispersion relations (c) and group velocities (d) in MAFO for magnons propagating (blue curves) along the [100] direction, (orange curves) along the [110] direction with the same exchange stiffness as for the blue curves, and (green curves) along the [110] direction with an exchange stiffness increased by 10%.

field. We do not observe deviations from the behavior $V_{SHE} \propto \cos(\phi)$ and $V_{SSE} \propto \cos^2(\phi)$ (Figure S1, Supporting Information) and therefore conclude that scattering time is not $\vec{k}$ orientation dependent.

We suggest, instead, that the anisotropy of our signal is dominated by anisotropies in the exchange energies associated with the MAFO crystal structure. Instead of assuming an isotropic exchange stiffness as in eqs 4–6, we can model the exchange stiffness D as a function of the orientation $\vec{k}$ relative to the crystal axes; more specifically, D is larger for $\vec{k}$ along the magnetic easy axis so as to increase group velocity in those directions. The results of a change in exchange stiffness on the magnon dispersion relation and group velocity are shown by the green curves in Figure 4c and d, which correspond to a 10% increase in exchange stiffness compared to the orange curves. In contrast to changes in magnetic anisotropy, a change in exchange stiffness has a significant impact throughout the Brillouin zone and not just in the immediate vicinity of $k = 0$. Since magnons throughout the Brillouin zone will be thermally excited at room temperature, we expect variations in exchange stiffness to have a larger impact on magnon propagation than changes in magnetic anisotropy for a uniform magnetic state.

The possibility of an anisotropic exchange stiffness has been considered theoretically.[39−41] For nonrelativistic exchange processes, the spin stiffness should not depend on the orientation of the magnetization with respect to the crystal axes (ϕ_H), but it can depend on the orientation of the wavevector relative to the crystal axes (ϕ_k). This is the symmetry required to explain our results without significant deviations from the observed dependence on the angle of magnetic field ($V_{SHE} \propto \cos(\phi)$ and $V_{SSE} \propto \cos^2(\phi)$).

The existence of anisotropy in exchange stiffness can also help to explain the differences in the magnitude of the spin transport signal extrapolated to small spacings d between source and detector wires—the fact that the spin signals in the limit of small d become larger for transport along the hard axis compared to the easy axis. The anisotropies in both the exchange stiffness and the energy of the uniform magnetic state have the sign to increase the energies of long-wavelength magnons with $\vec{k}$ along the easy axes, so the population of those magnons will be decreased relative to magnons with $\vec{k}$ along the hard axes.

Anisotropy in the exchange stiffness of bulk magnetic crystals has been measured previously by inelastic neutron scattering (e.g., ref 42), but we are not aware of previous studies sensitive to this type of anisotropy within epitaxial thin films. This is likely because the techniques most commonly used for measuring exchange stiffness in thin films, broadband ferromagnetic resonance[43,44] and Brillouin light scattering,[45,46] are sensitive primarily to exchange stiffness for wave vectors perpendicular to the film plane (through measurements of perpendicular standing spin wave modes), while the anisotropy we probe corresponds to different directions of in-plane wave vector.

CONCLUSION

In summary, we have measured magnon-mediated spin transport in epitaxially grown ultrathin (6 nm) $MgAl_{0.5}Fe_{1.5}O_4$ thin films. The small isotropic Gilbert damping parameter (∼0.0015) of these films, their soft magnetism (in-plane coercive field <0.5 mT), and low processing temperature (∼450 °C) make MAFO a particularly attractive platform for the study of magnon transport and integrated magnonic devices. Unlike previous studies of YIG samples, tetragonally strained epitaxial MAFO possesses substantial in-plane cubic magnetic anisotropy. We find also a strong anisotropy as a function of propagation direction in magnon-mediated spin transport, with spin diffusion lengths 30% larger along the easy axes as compared to that along the hard axes. The sign of this effect is opposite to what would be expected due simply to the magnetic anisotropy energy of a uniform magnetic state, so we suggest that the anisotropy in spin transport is dominated instead by anisotropy in exchange stiffness. An exchange stiffness that is larger for $\vec{k}$ along the magnetic easy axis can explain not only the longer spin diffusion lengths for transport along the easy axes but also larger nonlocal spin signals in the limit of small spacing that we observe for transport along the hard axes. Nonlocal spin wave transport measurements might therefore serve as a sensitive probe of exchange-stiffness anisotropy in thin-film samples. Since crystalline anisotropies can be tuned by strain, we also suggest that strain-mediated manipulation of exchange stiffness might provide a strategy for modulating spin transport in magnetic thin films.

Note Added: Following our paper, the Kläui group also found evidence of anisotropic exchange stiffness in the canted antiferromagnet $YFeO_3$.[47]

ASSOCIATED CONTENT

Supporting Information

The Supporting Information is available free of charge at https://pubs.acs.org/doi/10.1021/acs.nanolett.1c04332.

Sample growth and fabrication, nonlocal measurements of magnon spin transport, residuals in the angular fits, angular dependence along different axes, current dependence of the nonlocal voltage, ferromagnetic resonance measurements, atomic force microscopy (PDF)

AUTHOR INFORMATION

Corresponding Authors

Daniel C. Ralph − *Laboratory of Atomic and Solid-State Physics, Cornell University, Ithaca, New York 14853, United States; Kavli Institute at Cornell for Nanoscale Science, Ithaca, New York 14853, United States;* orcid.org/0000-0002-3026-0335; Email: dcr14@cornell.edu

Tianxiang Nan − *School of Integrated Circuits and Beijing National Research Center for Information Science and Technology (BNRist), Tsinghua University, Beijing 100084, China; Laboratory of Atomic and Solid-State Physics, Cornell University, Ithaca, New York 14853, United States;* Email: nantianxiang@mail.tsinghua.edu.cn

Authors

Ruofan Li − *Laboratory of Atomic and Solid State Physics, Cornell University, Ithaca, New York 14853, United States;* orcid.org/0000-0001-7746-9569

Peng Li − *Geballe Laboratory for Advanced Materials, Stanford University, Stanford, California 94305, United States;* orcid.org/0000-0001-8491-0199

Di Yi − *Geballe Laboratory for Advanced Materials, Stanford University, Stanford, California 94305, United States; State Key Lab of New Ceramics and Fine Processing, School of Materials Science and Engineering, Tsinghua University, Beijing 100084, China;* orcid.org/0000-0002-7209-1947

https://doi.org/10.1021/acs.nanolett.1c04332
Nano Lett. 2022, 22, 1167−1173

Lauren J. Riddiford − *Geballe Laboratory for Advanced Materials, Stanford University, Stanford, California 94305, United States; Department of Applied Physics, Stanford University, Stanford, California 94305, United States;* orcid.org/0000-0003-0941-7040

Yahong Chai − *School of Integrated Circuits and Beijing National Research Center for Information Science and Technology (BNRist), Tsinghua University, Beijing 100084, China*

Yuri Suzuki − *Geballe Laboratory for Advanced Materials, Stanford University, Stanford, California 94305, United States; Department of Applied Physics, Stanford University, Stanford, California 94305, United States*

Complete contact information is available at: https://pubs.acs.org/10.1021/acs.nanolett.1c04332

Notes

The authors declare no competing financial interest.

■ ACKNOWLEDGMENTS

We thank Andrei Slavin and Vasyl Tyberkevych for a critique of an initial draft of this paper and Satoru Emori, Jiamian Hu, Pu Yu, Dingfu Shao, and Evgeny Tsymbal for helpful discussions. Research at Cornell was supported by the Cornell Center for Materials Research with funding from the NSF MRSEC program (Grant No. DMR-1719 875). This work was performed in part at the Cornell NanoScale Facility, a member of the National Nanotechnology Coordinated Infrastructure, which is supported by the NSF (Grant No. NNCI-2025 233). Research at Tsinghua was supported by the National Natural Science Foundation (52 073 158,52 161 135 103), and the Beijing Advanced Innovation Center for Future Chip (ICFC). Research at Stanford was initially funded by a Vannevar Bush Faculty Fellowship of the Department of Defense (contract No. N00014-15-1-0045) and later by the Air Force Office of Scientific Research (Grant No. FA 9550-20-1-0293). L.J.R. also acknowledges support from an NSF Graduate Research Fellowship.

■ REFERENCES

(1) Chumak, A. V.; Vasyuchka, V. I.; Serga, A. A.; Hillebrands, B. Magnon spintronics. *Nat. Phys.* **2015**, *11*, 453−461.

(2) Adam, J. D. Analog signal processing with microwave magnetics. *Proceedings of the IEEE* **1988**, *76*, 159−170.

(3) Cornelissen, L. J.; Liu, J.; Duine, R. A.; Youssef, J. B.; van Wees, B. J. Long-distance transport of magnon spin information in a magnetic insulator at room temperature. *Nat. Phys.* **2015**, *11*, 1022−1026.

(4) Giles, B. L.; Yang, Z.; Jamison, J. S.; Myers, R. C. Long-range pure magnon spin diffusion observed in a nonlocal spin-Seebeck geometry. *Phys. Rev. B* **2015**, *92*, 224415.

(5) Shan, J.; Cornelissen, L. J.; Vlietstra, N.; Ben Youssef, J.; Kuschel, T.; Duine, R. A.; van Wees, B. J. Influence of yttrium iron garnet thickness and heater opacity on the nonlocal transport of electrically and thermally excited magnons. *Phys. Rev. B* **2016**, *94*, 174437.

(6) Collet, M.; Gladii, O.; Evelt, M.; Bessonov, V.; Soumah, L.; Bortolotti, P.; Demokritov, S. O.; Henry, Y.; Cros, V.; Bailleul, M.; Demidov, V. E.; Anane, A. Spin-wave propagation in ultra-thin YIG based waveguides. *Appl. Phys. Lett.* **2017**, *110*, 092408.

(7) Shan, J.; Bougiatioti, P.; Liang, L.; Reiss, G.; Kuschel, T.; van Wees, B. J. Nonlocal magnon spin transport in $NiFe_2O_4$ thin films. *Appl. Phys. Lett.* **2017**, *110*, 132406.

(8) Qin, H.; Hämäläinen, S. J.; Arjas, K.; Witteveen, J.; van Dijken, S. Propagating spin waves in nanometer-thick yttrium iron garnet films: Dependence on wave vector, magnetic field strength, and angle. *Phys. Rev. B* **2018**, *98*, 224422.

(9) Liu, C.; Chen, J.; Liu, T.; Heimbach, F.; Yu, H.; Xiao, Y.; Hu, J.; Liu, M.; Chang, H.; Stueckler, T.; Tu, S.; Zhang, Y.; Zhang, Y.; Gao, P.; Liao, Z.; Yu, D.; Xia, K.; Lei, N.; Zhao, W.; Wu, M.; et al. Long-distance propagation of short-wavelength spin waves. *Nat. Commun.* **2018**, *9*, 738.

(10) Liu, J.; Cornelissen, L. J.; Shan, J.; van Wees, B. J.; Kuschel, T. Nonlocal magnon spin transport in yttrium iron garnet with tantalum and platinum spin injection/detection electrodes. *J. Phys. D: Appl. Phys.* **2018**, *51*, 224005.

(11) Oyanagi, K.; Kikkawa, T.; Saitoh, E. Magnetic field dependence of the nonlocal spin Seebeck effect in Pt/YIG/Pt systems at low temperatures. *AIP Advances* **2020**, *10*, 015031.

(12) Demidov, V. E.; Urazhdin, S.; Anane, A.; Cros, V.; Demokritov, S. O. Spin−orbit-torque magnonics. *J. Appl. Phys.* **2020**, *127*, 170901.

(13) Goennenwein, S. T. B.; Schlitz, R.; Pernpeintner, M.; Ganzhorn, K.; Althammer, M.; Gross, R.; Huebl, H. Non-local magnetoresistance in YIG/Pt nanostructures. *Appl. Phys. Lett.* **2015**, *107*, 172405.

(14) Ganzhorn, K.; Wimmer, T.; Barker, J.; Bauer, G. E. W.; Qiu, Z.; Saitoh, E.; Vlietstra, N.; Geprägs, S.; Gross, R.; Huebl, H.; Goennenwein, S. T. B. Non-local magnon transport in the compensated ferrimagnet GdIG. *arXiv (Condensed Matter. Mesoscale and Nanoscale Physics)*. https://arxiv.org/abs/1705.02871 (accessed Jan 3, 2022).

(15) Schlitz, R.; Vélez, S.; Kamra, A.; Lambert, C.-H.; Lammel, M.; Goennenwein, S. T. B.; Gambardella, P. Control of Nonlocal Magnon Spin Transport via Magnon Drift Currents. *Phys. Rev. Lett.* **2021**, *126*, 257201.

(16) Lebrun, R.; Ross, A.; Bender, S. A.; Qaiumzadeh, A.; Baldrati, L.; Cramer, J.; Brataas, A.; Duine, R. A.; Kläui, M. Tunable long-distance spin transport in a crystalline antiferromagnetic iron oxide. *Nature* **2018**, *561*, 222−225.

(17) Xing, W.; Qiu, L.; Wang, X.; Yao, Y.; Ma, Y.; Cai, R.; Jia, S.; Xie, X. C.; Han, W. Magnon Transport in Quasi-Two-Dimensional van der Waals Antiferromagnets. *Phys. Rev. X* **2019**, *9*, 011026.

(18) Han, J.; Zhang, P.; Bi, Z.; Fan, Y.; Safi, T. S.; Xiang, J.; Finley, J.; Fu, L.; Cheng, R.; Liu, L. Birefringence-like spin transport via linearly polarized antiferromagnetic magnons. *Nat. Nanotechnol.* **2020**, *15*, 563−568.

(19) Cornelissen, L. J.; Shan, J.; van Wees, B. J. Temperature dependence of the magnon spin diffusion length and magnon spin conductivity in the magnetic insulator yttrium iron garnet. *Phys. Rev. B* **2016**, *94*, 180402.

(20) Ganzhorn, K.; Wimmer, T.; Cramer, J.; Schlitz, R.; Geprägs, S.; Jakob, G.; Gross, R.; Huebl, H.; Kläui, M.; Goennenwein, S. T. B. Temperature dependence of the non-local spin Seebeck effect in YIG/Pt nanostructures. *AIP Advances* **2017**, *7*, 085102.

(21) Gomez-Perez, J. M.; Vélez, S.; Hueso, L. E.; Casanova, F. Differences in the magnon diffusion length for electrically and thermally driven magnon currents in $Y_3Fe_5O_{12}$. *Phys. Rev. B* **2020**, *101*, 184420.

(22) Cornelissen, L. J.; Peters, K. J. H.; Bauer, G. E. W.; Duine, R. A.; van Wees, B. J. Magnon spin transport driven by the magnon chemical potential in a magnetic insulator. *Phys. Rev. B* **2016**, *94*, 014412.

(23) Cornelissen, L. J.; Liu, J.; van Wees, B. J.; Duine, R. A. Spin-Current-Controlled Modulation of the Magnon Spin Conductance in a Three-Terminal Magnon Transistor. *Phys. Rev. Lett.* **2018**, *120*, 097702.

(24) Das, K. S.; Feringa, F.; Middelkamp, M.; van Wees, B. J.; Vera-Marun, I. J. Modulation of magnon spin transport in a magnetic gate transistor. *Phys. Rev. B* **2020**, *101*, 054436.

(25) Cornelissen, L. J.; van Wees, B. J. Magnetic field dependence of the magnon spin diffusion length in the magnetic insulator yttrium iron garnet. *Phys. Rev. B* **2016**, *93*, 020403.

(26) Liu, J.; Wei, X.-Y.; Bauer, G. E. W.; Youssef, J. B.; van Wees, B. J. Electrically induced strong modulation of magnon transport in ultrathin magnetic insulator films. *Phys. Rev. B* **2021**, *103*, 214425.
(27) Emori, S.; Yi, D.; Crossley, S.; Wisser, J. J.; Balakrishnan, P. P.; Khodadadi, B.; Shafer, P.; Klewe, C.; N'Diaye, A. T.; Urwin, B. T.; Mahalingam, K.; Howe, B. M.; Hwang, H. Y.; Arenholz, E.; Suzuki, Y. Ultralow Damping in Nanometer-Thick Epitaxial Spinel Ferrite Thin Films. *Nano Lett.* **2018**, *18*, 4273−4278.
(28) Wisser, J. J.; Emori, S.; Riddiford, L.; Altman, A.; Li, P.; Mahalingam, K.; Urwin, B. T.; Howe, B. M.; Page, M. R.; Grutter, A. J.; Kirby, B. J.; Suzuki, Y. Ultrathin interfacial layer with suppressed room temperature magnetization in magnesium aluminum ferrite thin films. *Appl. Phys. Lett.* **2019**, *115*, 132404.
(29) Wisser, J. J.; Grutter, A. J.; Gilbert, D. A.; N'Diaye, A. T.; Klewe, C.; Shafer, P.; Arenholz, E.; Suzuki, Y.; Emori, S. Damping Enhancement in Coherent Ferrite−Insulating-Paramagnet Bilayers. *Phys. Rev. Applied* **2019**, *12*, 054044.
(30) Wisser, J. J.; Riddiford, L. J.; Altman, A.; Li, P.; Emori, S.; Shafer, P.; Klewe, C.; N'Diaye, A. T.; Arenholz, E.; Suzuki, Y. The role of iron in magnetic damping of $Mg(Al,Fe)_2O_4$ spinel ferrite thin films. *Appl. Phys. Lett.* **2020**, *116*, 142406.
(31) Riddiford, L. J.; Wisser, J. J.; Emori, S.; Li, P.; Roy, D.; Cogulu, E.; van 't Erve, O.; Deng, Y.; Wang, S. X.; Jonker, B. T.; Kent, A. D.; Suzuki, Y. Efficient spin current generation in low-damping $Mg(Al,Fe)_2O_4$ thin films. *Appl. Phys. Lett.* **2019**, *115*, 122401.
(32) Vila, L.; Kimura, T.; Otani, Y. Evolution of the Spin Hall Effect in Pt Nanowires: Size and Temperature Effects. *Phys. Rev. Lett.* **2007**, *99*, 226604.
(33) Uchida, K.; Takahashi, S.; Harii, K.; Ieda, J.; Koshibae, W.; Ando, K.; Maekawa, S.; Saitoh, E. Observation of the spin Seebeck effect. *Nature* **2008**, *455*, 778−781.
(34) Saitoh, E.; Ueda, M.; Miyajima, H.; Tatara, G. Conversion of spin current into charge current at room temperature: Inverse spin-Hall effect. *Appl. Phys. Lett.* **2006**, *88*, 182509.
(35) Jungfleisch, M. B.; Chumak, A. V.; Kehlberger, A.; Lauer, V.; Kim, D. H.; Onbasli, M. C.; Ross, C. A.; Kläui, M.; Hillebrands, B. Thickness and power dependence of the spin-pumping effect in $Y_3Fe_5O_{12}$/Pt heterostructures measured by the inverse spin Hall effect. *Phys. Rev. B* **2015**, *91*, 134407.
(36) Kalinikos, B. A.; Kostylev, M. P.; Kozhus, N. V.; Slavin, A. N. The dipole-exchange spin wave spectrum for anisotropic ferromagnetic films with mixed exchange boundary conditions. *J. Phys.: Condens. Matter* **1990**, *2*, 9861−9877.
(37) McMichael, R. D.; Krivosik, P. Classical model of extrinsic ferromagnetic resonance linewidth in ultrathin films. *IEEE Trans. Magn.* **2004**, *40*, 2−11.
(38) Sekiguchi, K.; Lee, S.-W.; Sukegawa, H.; Sato, N.; Oh, S.-H.; McMichael, R. D.; Lee, K.-J. Spin-wave propagation in cubic anisotropic materials. *NPG Asia Materials* **2017**, *9*, e392−e392a.
(39) Belashchenko, K. Anisotropy of exchange stiffness and its effect on the properties of magnets. *J. Magn. Magn. Mater.* **2004**, *270*, 413−424.
(40) Skomski, R.; Kashyap, A.; Zhou, J.; Sellmyer, D. J. Anisotropic exchange. *J. Appl. Phys.* **2005**, *97*, 10B302.
(41) Heide, M.; Bihlmayer, G.; Blügel, S. Dzyaloshinskii-Moriya interaction accounting for the orientation of magnetic domains in ultrathin films: Fe/W(110). *Phys. Rev. B* **2008**, *78*, 140403.
(42) Naser, H.; Rado, C.; Lapertot, G.; Raymond, S. Anisotropy and temperature dependence of the spin-wave stiffness in $Nd_2Fe_{14}B$: An inelastic neutron scattering investigation. *Phys. Rev. B* **2020**, *102*, 014443.
(43) Schreiber, F.; Frait, Z. Spin-wave resonance in high-conductivity films: The Fe-Co alloy system. *Phys. Rev. B* **1996**, *54*, 6473−6480.
(44) Klingler, S.; Chumak, A. V.; Mewes, T.; Khodadadi, B.; Mewes, C.; Dubs, C.; Surzhenko, O.; Hillebrands, B.; Conca, A. Measurements of the exchange stiffness of YIG films using broadband ferromagnetic resonance techniques. *J. Phys. D: Appl. Phys.* **2015**, *48*, 015001.
(45) Hamrle, J.; Gaier, O.; Min, S.-G.; Hillebrands, B.; Sakuraba, Y.; Ando, Y. Determination of exchange constants of Heusler compounds by Brillouin light scattering spectroscopy: application to Co_{2MnSi}. *J. Phys. D: Appl. Phys.* **2009**, *42*, 084005.
(46) Haldar, A.; Banerjee, C.; Laha, P.; Barman, A. Brillouin light scattering study of spin waves in NiFe/Co exchange spring bilayer films. *J. Appl. Phys.* **2014**, *115*, 133901.
(47) Das, S. et al. Anisotropic long-range spin transport in canted antiferromagnetic orthoferrite $YFeO_3$. *arXiv (Condensed Matter. Strongly Correlated Electrons)*. https://arxiv.org/abs/2112.05947 (accessed Jan 3, 2022).

https://doi.org/10.1021/acs.nanolett.1c04332
Nano Lett. 2022, 22, 1167−1173